RESEARCH INTO ADVANCED CONCEPTS OF MICROWAVE POWER AMPLIFICATION AND GENERATION UTILIZING LINEAR BEAM DEVICES

P. R. McIsaac
School of Electrical Engineering
Cornell University

Final Status Report
December 1972

Research Grant NGL 33-010-047 No. 2
National Aeronautics and Space Administration
Office of Grants and Research Contracts
Code SC
Washington, D. C. 20546

ABSTRACT

This is a final report which summarizes the work performed on this research grant from November 1966 to November 1972. This project was a theoretical study of some aspects of the interaction between a drifting stream of electrons with transverse cyclotron motions and an electromagnetic field. Particular emphasis was given to the possible generation and amplification of millimeter waves. The major effort during this project was devoted to a theoretical study of the cyclotron resonance oscillator. The appendices include published papers on the cyclotron resonance oscillator which resulted from this investigation.

TABLE OF CONTENTS

I. INTRODUCTION

The objective of this research program is to explore theoretically some aspects of the interaction between a drifting stream of electrons having transverse cyclotron motions and an electromagnetic field; particularly emphasis being given to the possible generation and amplification of millimeter waves. Because of this interest in possible applications to millimeter wavelengths, this study concentrates on electron stream-electromagnetic field interactions which involve a uniform, or fast-wave, circuit structure or cavity of simple shape.

This report briefly summarizes the work performed on this grant since its start in November 1966. The major effort during this period was devoted to a theoretical study of the cyclotron resonance oscillator. This included the development of a coupled mode analysis of the interaction between the electron beam and the electromagnetic fields of the cavity, a study of the start oscillation conditions for a cyclotron resonance oscillator, and a large signal ballistic analysis of the saturation effects in a cyclotron resonance oscillator which limit its efficiency. Other minor studies performed on this grant are also summarized. The appendices include three published papers on the cyclotron resonance oscillator which resulted from this investigation.

II. REVIEW OF THE PROJECT

Since its inception in November, 1966, this project has been concerned with the study of the interaction between an electron stream and the electromagnetic field of a uniform structure. In particular, the study has concentrated primarily on the interaction between a drifting stream of electrons with transverse cyclotron motions and the electromagnetic field of a fast-wave circuit. The objective motivating this choice of subject for investigation was to explore the cyclotron resonance oscillator, including the underlying physical principles which cause the oscillation, the electron beam and circuit parameters which determine the performance, and the nonlinear effects which limit the performance. This investigation of the cyclotron resonance oscillator is believed to be the most comprehensive theoretical study of the device that has been made.

The basic components of the cyclotron resonance oscillator are a spiraling electron beam and a cavity through which the electron beam drifts. An axial d-c magnetic field is applied to the electron beam to focus it; this magnetic field determines the rotation frequency of the electrons as they spiral through the device. It is found that when the relativistic cyclotron frequency of the electron beam is adjusted to be slightly lower than the resonant frequency of the cavity (for a mode with strong transverse electric fields),

oscillation will occur if the d-c beam current magnitude and cavity loaded Q are properly adjusted. Of course, an appropriate electron gun to launch the electron beam and a collector to terminate the electron beam are necessary components of the device; however, since these elements do not enter into the interaction process they have not been studied on this project. This device is of interest for millimeter wave generation because of the simple physical form that the cavity interaction region can be given.

Major effort during the project was devoted to the study of the interaction between a spiraling filamentary electron beam and the electromagnetic fields of a uniform waveguide or cavity. This restriction to a filamentary electron beam makes the analysis much more tractable. The study was divided into three sections. In the first part of the study the coupled mode equations for a spiraling filamentary electron beam drifting through a uniform waveguide were derived. The spiraling filamentary electron beam has six modes: two cyclotron waves, two synchronous waves, and two (degenerate) space charge waves. Four modes of the uniform waveguide were considered: positive and negative circularly polarized waves (TE or TEM) traveling parallel and anti-parallel to the direction of the electron beam drift. The coupled mode equations describe the interaction between these ten waves.

One important conclusion of this study is that relativistic effects, including both the electrons' mass variation with velocity and the a-c magnetic force acting on the electrons (in addition to the a-c electric force) are important in the interaction. In particular, the mass variation with velocity is necessary to explain the occurrence of amplification or oscillation in a spiraling electron beam device. The development of these coupled mode equations is discussed in the Semiannual Status Reports of December 1967, June 1968, and December 1968; see also Appendix I.

In the second part of the study, the start oscillation conditions for a cyclotron resonance oscillator employing a spiraling filamentary electron beam drifting through a half wavelength rectangular cavity of square cross section were investigated. A digital computer was used to solve the ten simultaneous equations resulting from the coupled mode description of the interaction between the six electron beam waves and the four circuit waves. It was found that the d-c electron beam current required for start oscillation varies approximately inversely with the loaded Q of the cavity, Q_L. The dependence of the start oscillation condition on the ratio of the length-to-width of the cavity at fixed d-c electron beam current and cavity Q_L was explored, as well as the sensitivity to the axial d-c electron drift velocity. Also, the dependence of the start oscillation frequency on

the d-c electron beam current and the ratio of the length-to-width of the cavity was examined. The start oscillation conditions for the cyclotron resonance oscillator are discussed in the Semiannual Status Reports of July 1969, June 1970 and December 1970; see also Appendix II.

The third part of the study was the development of a large signal ballistic theory for the cyclotron resonance oscillator. Digital computer calculations based on this large signal theory were made to explore the nonlinear effects which may limit the saturation power output and efficiency attainable in a cyclotron resonance oscillator. These large signal calculations again indicated the importance of the relativistic mass dependence on the velocity of the electrons as the major gain mechanism in the device. Although the device is electrically short (one-half wavelength), the electron beam response under oscillating conditions is extremely nonlinear with electron cross-overs occurring in the cavity interaction region. It is concluded that for typical electron beam and cavity parameters, device efficiencies of the order of 4 - 5% may be expected. The large signal theory for cyclotron resonance oscillators is discussed in the Semiannual Status Reports of June 1971 and December 1971; see also Appendix III.

In addition to this major effort devoted to the study of the interaction between a spiraling filamentary electron beam

and the electromagnetic fields of a uniform waveguide or cavity, several other related, but minor, studies were undertaken during the course of the project. One of these was the development of the coupled mode equations for a spiraling hollow electron beam drifting through a uniform waveguide. This is discussed in the Semiannual Status Reports of July 1969 and December 1971. A fairly detailed investigation of the focusing of relativistic electron beams was also made; see the Semiannual Status Reports of May 1967 and December 1967.

Finally, work was initiated on the application of symmetry analysis to the study of electron beam-electromagnetic field interaction. The first effort involved the combination of some aspects of group theory with coupled mode theory to investigate the space charge waves on a system of several electron beams in parallel. (See the Semiannual Status Report of June 1970). More recently, the space groups for structures with an axis of symmetry (these groups are called stem groups) have been investigated. In particular, the stem groups appropriate to periodic electron beams were studied. This represents a beginning to a major development of the application of symmetry analysis to electron beam devices. This work is discussed in the Semiannual Status Report of August 1972.

APPENDIX I

SPIRALING ELECTRON BEAM INTERACTION WITH FAST WAVE CIRCUITS

P. R. McIsaac

(Proceedings of the 7th International Conference on Microwave and Optical Generation and Amplification, MOGA 68, VDE-Verlag GMBH, Berlin, 1968)

SPIRALING ELECTRON BEAM INTERACTION WITH FAST WAVE CIRCUITS

P. R. McIsaac, Ithaca, New York

Cornell University

0. SUMMARY

A small signal, coupled mode theory including relativistic effects is developed to analyze the interaction between spiraling electron beams and uniform fast wave circuits. The six normal modes of a spiraling filamentary electron beam together with the four normal modes of a TEM circuit are defined. Typical ω-β diagrams are presented, and the interaction of the coupled system and the possibility of amplification are discussed.

1. INTRODUCTION

The interaction between spiraling electron beams and uniform fast wave circuits is potentially important as a method of generating and amplifying millimeter waves. The method is attractive because of the simplicity of the interaction circuit and because of the possibility of tuning the device by controlling the axial d-c magnetic field (which determines the pitch of the helical electron motion). Recently several devices using the interaction between a spiraling electron beam and a fast wave circuit have been investigated. [1,2,3,4,5,6,7]

This paper presents a small signal, coupled mode analysis of the interaction between a spiraling electron beam and the electromagnetic fields of a fast wave circuit. The objective is to present a theory which is sufficiently simple to provide a clear physical interpretation of the interaction mechanism, but which is also sufficiently detailed to provide relevant design data and information concerning the influence of the important electron beam and circuit parameters.

To ensure the requisite simplicity for the analysis, a filamentary electron beam is taken as the model for the spiraling electron beam. In addition, this enables the analysis to be compared with the previously established results[8] in the limiting case of a straight filamentary electron beam.

2. COUPLED MODE EQUATIONS

The filamentary electron beam is shown schematically in Fig. 1. The helical d-c motion of the electron beam is maintained by the axial d-c magnetic flux density B_o. The electrons spiral about the z axis with a radius r_o, constant angular velocity $\dot{\theta}_o = \eta\omega_c$, and constant axial velocity $\dot{z}_o$. The angular velocity is equal to the relativistic cyclotron frequency with $\omega_c = eB_o/m$ and $\eta = [1-(v_o/c)^2]^{1/2}$; $-e$ is the charge and m is the rest mass of an electron, v_o is the d-c beam velocity, and c is the velocity of light. The pitch of

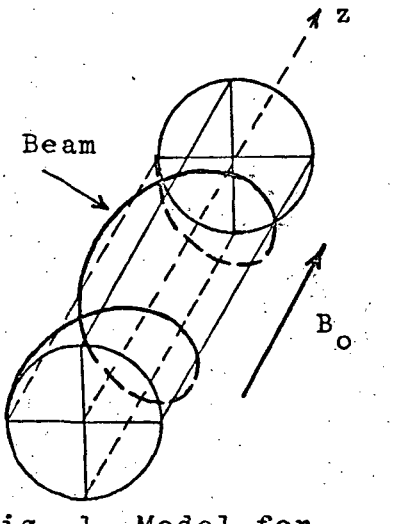

Fig. 1. Model for spiraling filamentary electron beam.

This research was supported by NASA, Electronics Research Center, Cambridge, Mass.

the beam spiral is $2\pi\tilde{z}_o/\eta\omega_c = 2\pi/\eta\beta_c$.

Because of the possibility of r-f displacements and velocities in three coordinate directions, there will be six beam waves. Three of the beam equations come from the relativistic equations of motion for the electrons; these can be written vectorially as

$$\frac{d}{dt}\left[\frac{\bar{v}}{[1-(v/c)^2]^{1/2}}\right] = -\frac{e}{m}(\bar{E} + \bar{v}x\bar{B}) + \omega_c(\bar{a}_z x\bar{v}). \tag{1}$$

Here, $\bar{E}$ and $\bar{B}$ are the a-c electric field and magnetic flux density of the electromagnetic wave interacting with the electrons, and $\bar{a}_z$ is a unit vector in the z direction.

These equations are nonlinear; to convert them to a form appropriate for a small signal analysis, the velocity is expressed as the sum of an unperturbed part $\bar{v}_o$ and an r-f perturbation $\bar{v}_1$ which is assumed to be small, $|\bar{v}_1^o| << |\bar{v}_o|$. Using a binomial expansion for the square root, the small signal equations of motion are obtained by retaining only the first order terms in the r-f perturbation.

$$\frac{d}{dt}\left[\frac{\bar{v}_1}{\eta} + \frac{\bar{v}_o(\bar{v}_o.\bar{v}_1)}{c^2\eta^3}\right] = -\frac{e}{m}(\bar{E} + \bar{v}_o x\bar{B}) + \omega_c(\bar{a}_z x\bar{v}_1) \tag{2}$$

The remaining three equations for the beam are the equations relating the r-f velocities to the r-f displacements;

$$\frac{d\bar{r}_1}{dt} = \bar{v}_1 . \tag{3}$$

In general there will be four circuit waves for each waveguide mode which interacts with the beam; these include both senses of circular polarization for each of the two directions of propagation ($\pm z$). Maxwell's curl equations supply the four equations for the circuit waves. For simplicity, attention will be confined here to TEM waves, and the circuit equations can be written as

$$[\bar{a}_z x \frac{\partial\bar{E}}{\partial z}] + jkZ\bar{H} = 0, \tag{4a}$$

$$Z[\bar{a}_z x \frac{\partial\bar{H}}{\partial z}] - jk\bar{E} = -\frac{ZI_o}{A\tilde{z}_o}\bar{v}_1, \tag{4b}$$

where $k = \omega/c$ is the phase constant for a TEM wave, $Z=(\mu/\varepsilon)^{1/2}$ is the impedance of free space, A is the cross sectional area of the circuit, and I_o is the d-c beam current along the spiral. Extension to the TE or TM modes of an uniform waveguide is without difficulty.

As in the case of a straight filamentary electron beam, it is convenient to introduce circularly polarized components for the r-f displacements, velocities, and electromagnetic fields. However, in the spiraling beam case, to facilitate transforming to normal mode form, it is necessary to introduce an additional phase shift into the circularly polarized components. We define:

$$r'_{\pm} = r_{\pm}e^{\mp j\eta\beta_c z} = (x_1 \pm jy_1)e^{\mp j\eta\beta_c z}, \tag{5a}$$

$$u'_{\mp} = u_{\mp} e^{\mp j\eta\beta_c z} = (\dot{x}_1 \mp j\dot{y}_1)e^{\mp j\eta\beta_c z}, \tag{5b}$$

with corresponding equations for the circularly polarized components of the electric and magnetic fields.

Equations (2), (3), and (4) provide the ten coupled mode equations for the interaction between the spiraling electron beam and the TEM circuit. For the coupled mode analysis, it is necessary to choose appropriate waves which are eigenvectors of the uncoupled systems. For the circuit waves, an appropriate choice is

$$F'_{\mp} = \sqrt{\frac{A}{8Z}}\,(E'_{\mp} \mp jZH'_{\mp}), \tag{6a}$$

$$G'_{\mp} = \sqrt{\frac{A}{8Z}}\,(E'_{\mp} \pm jZH'_{\mp}). \tag{6b}$$

The F'_+ and F'_- waves correspond to propagation in the +z direction and the G'_+ and G'_- waves to propagation in the -z direction. This choice of normalization causes the power in the +z direction associated with the various circuit waves to be: $F'_+F'^*_+/2$, $F'_-F'^*_-/2$, $-G'_+G'^*_+/2$ and $-G'_-G'^*_-/2$ respectively.

An appropriate choice of eigenvectors for the six beam waves is

$$P'_+ = C(u'_+ + u'_-), \tag{7a}$$

$$P'_- = C(u'_+ - u'_- + j\frac{2\sigma}{\eta\zeta}\dot{z}_1), \tag{7b}$$

$$Q'_+ = C[(1+\zeta^2/2)u'_+ - \zeta^2 u'_-/2 - j\eta\omega_c r'_+ + j\frac{\sigma\zeta}{\eta}\dot{z}_1], \tag{7c}$$

$$Q'_- = C[(1+\zeta^2/2)u'_- - \zeta^2 u'_+/2 + j\eta\omega_c r'_- - j\frac{\sigma\zeta}{\eta}\dot{z}_1], \tag{7d}$$

$$V = C\frac{2}{\eta\zeta}\dot{z}_1, \tag{7e}$$

$$W = C\frac{2\omega_c}{\zeta}z_1, \tag{7f}$$

with $C = (mI_o/8e\eta)^{1/2}$, $\sigma = \dot{z}_o/c$, and $\zeta = \omega_c r_o/c$.

The ten coupled mode equations for the interaction between a spiraling filamentary electron beam and a TEM circuit are:

$$(\frac{\partial}{\partial z} + j\beta_e)P'_+ + j\eta\beta_c\zeta^2 P'_- + K[(1-\sigma)(F'_+ + F'_-) + (1+\sigma)(G'_+ + G'_-)] = 0, \tag{8a}$$

$$(\frac{\partial}{\partial z} + j\beta_e)P'_- + \eta^2 K[F'_+ - F'_- + G'_+ - G'_-] = 0, \tag{8b}$$

$$(\frac{\partial}{\partial z} + j\beta_e + j\eta\beta_c)Q'_+ + K[(1-\sigma)F'_+ + (1+\sigma)G'_+] = 0, \tag{8c}$$

$$(\frac{\partial}{\partial z} + j\beta_e - j\eta\beta_c)Q'_- + K[(1-\sigma)F'_- + (1+\sigma)G'_-] = 0, \tag{8d}$$

$$(\frac{\partial}{\partial z} + j\beta_e)V - jK[(1-\sigma)(F'_+ - F'_-) - (1+\sigma)(G'_+ - G'_-)] = 0, \tag{8e}$$

$$(\frac{\partial}{\partial z} + j\beta_e)W - \eta\beta_c V = 0, \tag{8f}$$

$$(\frac{\partial}{\partial z} + jk + j\eta\beta_c)F'_+ - K[P'_+ + P'_- - j\sigma V] = 0, \tag{8g}$$

$$\left(\frac{\partial}{\partial z} + jk - j\eta\beta_c\right)F_-' - K[P_+' - P_-' + j\sigma V] = 0, \tag{8h}$$

$$\left(\frac{\partial}{\partial z} - jk + j\eta\beta_c\right)G_+' + K[P_+' + P_-' - j\sigma V] = 0, \tag{8i}$$

$$\left(\frac{\partial}{\partial z} - jk - j\eta\beta_c\right)G_-' + K[P_+' - P_-' + j\sigma V] = 0, \tag{8j}$$

with $\beta_e = \omega/\dot{z}_o = k/\sigma$. The coupling constant K is given by $K = (\eta e I_o Z/mA)^{1/2}/2\dot{z}_o$.

3. SPIRALING BEAM INTERACTION

The ω-β diagram for the six beam waves and four circuit waves in the case of zero coupling (K = 0) is shown in Fig. 2. Note that this diagram is for the eigenvectors of the system and includes the phase shifts of $\mp\eta\beta_c z$ for the positive and negative circularly polarized components.

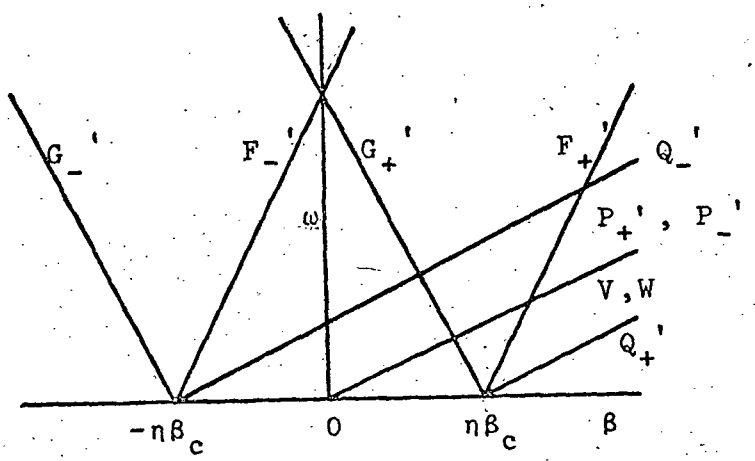

Fig. 2. The ω-β diagram for an uncoupled spiraling electron beam and TEM circuit.

Equations (8) indicate that for K = 0, certain of the beam waves are coupled together. For example,

$$V = V_o e^{-j\beta_e z}, \tag{9a}$$

$$W = W_o e^{-j\beta_e z} + \eta\beta_c z V. \tag{9b}$$

This is a consequence of the lack of a restoring force for the beam in the z direction in this model (the filamentary electron beam neglects space charge forces). Any initial r-f velocity in the z direction will produce an r-f displacement which grows linearly with distance.

Also, P_+' and P_-' are coupled together when K = 0.

$$P_+' = P_{+o}' e^{-j\beta_e z} - j\eta\beta_c z\, \zeta^2 P_-' \tag{10a}$$

$$P_-' = P_{-o}' e^{-j\beta_e z} \tag{10b}$$

Both of these waves are related to the r-f velocity in the transverse plane (for V = 0). The coupling of these waves indicates that the isolated spiraling beam is unstable as far as transverse velocities are concerned, although the growth of the P_+' wave is slow. It also indicates that it is impossible to maintain only a single circularly polarized velocity wave (either u_+ or u_-) on the isolated spiraling beam. If one is excited, then it couples to the other and eventually, downstream, both are equal in magnitude and grow linearly with distance.

The Q'_+ and Q'_- beam waves and the F'_- and G'_- circuit waves will not interact appreciably with the other waves, because their phase velocities are too widely separated. However, there is the possibility of significant interaction between the remaining four beam waves, P'_+, P'_-, V, W, and two circuit waves F'_+, G'_+, in the neighborhood of the intersections of these waves in Fig. 2; that is, at $\beta_e = \eta\beta_c \pm k$. Assuming that the waves have an exponential z dependence, $\exp(-j\beta z)$, the six wave interaction leads to the following polynomial for the six possible phase constants:

$$(\beta-\beta_e)^2\{(\beta-\beta_e)^4 + 2(\beta_e-\eta\beta_c)(\beta-\beta_e)^3 \tag{11}$$

$$-[k^2-(\beta_e-\eta\beta_c)^2 - 4\sigma K^2](\beta-\beta_e)^2$$

$$-2K^2[k(1+\eta^2+\sigma^2) - 2\sigma(\beta_e-\eta\beta_c)](\beta-\beta_e) - 2\eta^3\beta_c\zeta^2K^2k\} = 0$$

Clearly there is a double root at $\beta=\beta_e$. At the lower intersection $\beta_e=\eta\beta_c-k$, two of the remaining roots are real and the other two roots are complex conjugates, for all values of K. At the upper intersection, $\beta_e=\eta\beta_c+k$, all of the remaining four roots are real, at least for a wide range of parameter values. The ω-β diagram for the six wave coupled system is shown in Fig. 3 for a typical value of the coupling constant K (the dotted curve represents imaginary values of β).

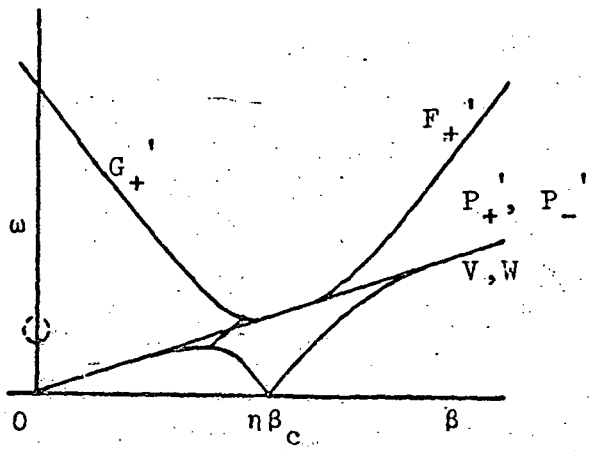

Fig. 3. The ω-β diagram for a coupled spiraling electron beam and TEM circuit.

This coupled mode analysis predicts that amplification can be produced by the interaction between a spiraling electron beam and a TEM circuit. For example, a specific amplifier configuration is shown schematically in Fig. 4. The input wave is G'_{+c}, and the output wave is G'_{+a}. In the interaction region (region b) there are the six waves mentioned above: F'_{+b}, G'_{+b}, P'_{+b}, P'_{-b}, V_b, and W_b. Each of these waves has several components, with each component characterized by one of the phase constants which is a solution of (11). For a given set of electron beam and circuit parameters, the solutions of (11), together with the boundary conditions at the input and output, permit the determination of the gain, G'_{+a}/G'_{+c}, of the device. The appropriate boundary conditions are: (1) continuity of the electric and magnetic fields at z = 0,L, and (2) the absence of r-f displacements and velocities on the electron beam at z = 0. One finds that over a suitable range of parameters, there will be a net electronic gain for this interaction.

The presence of six waves in the interaction region means that any explanation of the amplification in terms of the coupling between waves must be fairly complex. However, in comparing this interaction of a spiraling filamentary electron beam to that of a straight filamentary electron beam, a major difference here is the coupling between the P'_+ and P'_- waves and the V wave (in the

presence of a TEM circuit wave). That is, the r-f velocities in the transverse plane and the axial direction are all coupled together because of the beam spiraling. Further study of this interaction should clarify the amplification mechanism, as well as indicate the optimum ranges for the electron beam and circuit parameters.

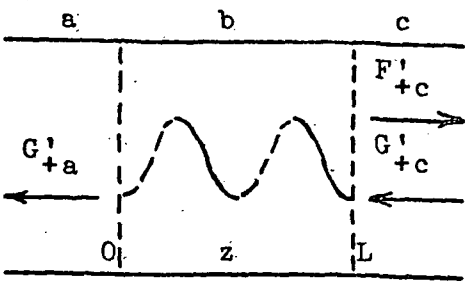

Fig. 4. Amplifier configuration for spiraling electron beam - TEM circuit interaction.

REFERENCES

[1] Pantell,R.H.: Electron Beam Interaction with Fast Waves. Proc. Symp. on Millimeter Waves, New York (1959) pp 301-311.

[2] Beck,A.H.W. and Mayo,R.F.: Interaction of an Electron Beam with the High-Order Modes of a Smooth Waveguide. Proc. 3rd Int. Conf. on Microwave Tubes, Munich (1960) pp 240-241.

[3] Bott,I.B.: Tunable Source of Millimeter and Submillimeter Electromagnetic Radiation. Proc. IRE 52 (1964) pp 330-332.

[4] Hirshfield, J.L. and Wachtel, J.M.: Electron Cyclotron Maser. Phys. Rev. Letters 12 (1964) pp 533-536.

[5] Schriever,R.L. and Johnson,C.C.: A Rotating Beam Waveguide Oscillator, Proc. IEEE 54 (1966) pp 2029-2030.

[6] Anatakov,I.I., Gaponov,A.V., Malygin,O.V., and Flyagin,V.A.: Application of Induced Cyclotron Radiation of Electrons for the Generation and Amplification of High-Powered Electromagnetic Waves. Radio Engr. and Elect. Phys. 11 (1966) pp 1995-1998.

[7] Beasley,J.P.: An Electron Cyclotron Resonance Oscillator at Millimetre Wavelengths. Proc. 6th Int. Conf. on Microwave and Optical Generation and Amplification, Cambridge (1966) pp 132-139.

[8] Siegman,A.E.: Waves on a Filamentary Electron Beam in a Transverse-Field Slow-Wave Circuit. J.Appl. Phys. 31 (1960) pp 17-26.

APPENDIX II

START OSCILLATION CONDITIONS FOR CYCLOTRON RESONANCE OSCILLATORS

P. R. McIsaac and J. F. Rowe, Jr.

(Proceedings of the 8th International Conference on Microwave and Optical Generation and Amplification MOGA 70, Kluwer-Devanter, The Netherlands, 1970)

START OSCILLATION CONDITIONS FOR CYCLOTRON RESONANCE OSCILLATORS

P. R. McIsaac and J. F. Rowe, Jr.
Cornell University, Ithaca, New York 14850, U.S.A.

1. Introduction

The cyclotron resonance oscillator utilizes the interaction between the electromagnetic fields of a cavity and a spiraling electron beam drifting through the cavity along a longitudinal magnetic field. The interaction can produce an oscillation at a frequency close to the relativistic cyclotron frequency of the electrons. This paper describes the use of a small signal, coupled mode analysis to determine the start oscillation conditions for the cyclotron resonance oscillator. The dependence of the start oscillation beam current on the loaded Q and dimensions of the cavity, and on the d-c magnetic flux density B_o is discussed for typical beam and cavity parameters.

The model employed for this analysis assumes a spiraling filamentary electron beam drifting through a rectangular cavity of square cross section (height = width = a) with its length L adjusted so that the TE_{101} resonant frequency is close to the cyclotron frequency. Relativistic effects are included in the analysis; that is, magnetic as well as electric forces on the electrons are considered, and dependence of the electron mass on the velocity is included. Space charge forces are neglected. For the physical details of experimental cyclotron resonance oscillators, reference may be made to the literature.[1,2,3,4]

2. Coupled mode theory

A coupled mode theory for the interaction between a spiraling filamentary electron beam and the electromagnetic fields of an uniform waveguide was reported previously.[5] The circuit has four waves (positive and negative circularly polarized waves in both the forward and reverse directions), while the electron beam has six waves. The beam waves can be labeled by their characteristic form in the limiting case of a straight filamentary electron beam: two cyclotron waves, two synchronous waves, and two (degenerate) space charge waves. It was found that significant interaction occurs between six of these waves; the forward and reverse, positive circularly polarized, circuit waves, and the two cyclotron and two degenerate space charge waves of the electron beam.

Figure 1 shows the ω-β diagram for these six waves in the coupled system. It should be noted that the curves for the two circuit waves and the two cyclotron waves have been shifted horizontally by $n\beta_c$; this simplifies the form of the coupled mode equations and their solutions in the spiraling electron beam case. Here, $n=(1-(v_o/c)^2)^{\frac{1}{2}}$ and $\beta_c = \omega_c/v_{oz}$, where $\omega_c = eB_o/m_o$ is the non-relativistic cyclotron frequency. Note that there is a pair of waves with complex conjugate propagation constants in the coupled system at both the lower and upper intersection points of the uncoupled system. How-

ever, it is found that amplification or oscillation occurs only in the neighborhood of the upper intersection point.

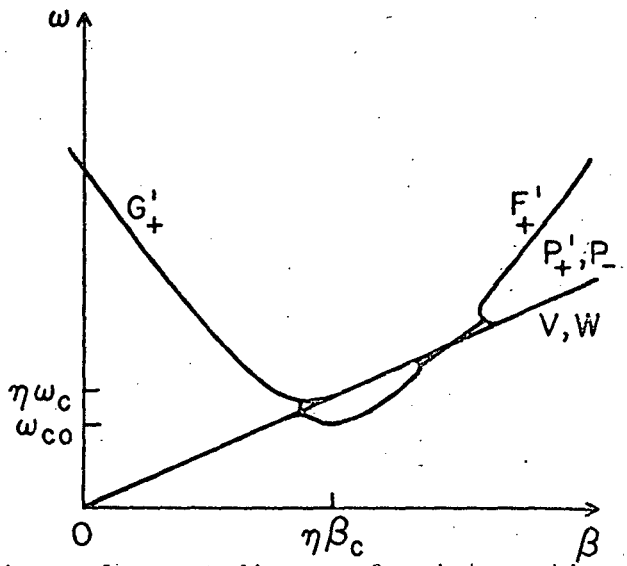

Figure 1. ω-β diagram for interaction between a spiraling filamentary electron beam and a waveguide. F'_+, G'_+ are positive circularly polarized circuit waves; P'_+, P'_- are beam cyclotron waves; V, W are beam (degenerate) space charge waves.

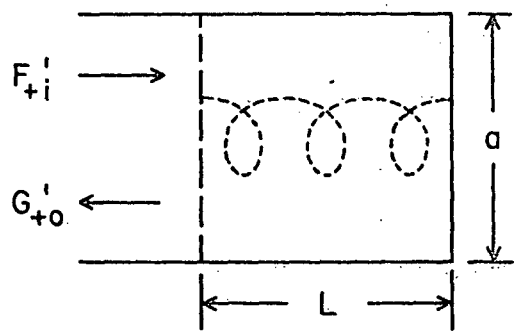

Figure 2. Schematic Diagram of a cyclotron resonance oscillator.

The start oscillation calculations are based on this coupled mode theory which is applied to the one-port amplifier shown in Figure 2. The interaction space is a half wavelength cavity shorted at the right, through which the spiraling electron beam drifts from left to right. On the left, an input wave F'_{+i} which is positive circularly polarized relative to B_o is incident on the interaction region, and the output circuit wave G'_{+o}, also positive circularly polarized relative to B_o, propogates to the left. The various circuit and beam parameters are adjusted until the amplifier gain G'_{+o}/F'_{+i} is infinite; this determines the start oscillation condition.

The electron beam parameters are the normalized axial and transverse velocities, $\sigma = v_{oz}/c$ and $\zeta = \eta\omega_c r_o/c$ (where r_o is the d-c beam radius), and the d-c beam current I_o. The cavity parameters, in addition to L and a, are Q_o, Q_x, and Q_L. Losses in the cavity walls are included, with Q_o adjusted to account for copper walls. In this model Q_x is varied by changing the assumed characteristic impedance of the output waveguide.

The general form for the solution of six coupled mode equations is known. For a given set of parameter values, a digital computer is used to evaluate the propagation constants for the coupled waves (in the neighborhood of the upper intersection point on the ω-β diagram) and to evaluate the wave amplitudes and phases which are fixed by the boundary conditions. Then the computer calculates the gain G'_{+o}/F'_{+i}, for the one-port amplifier. The parameter values that must be chosen are σ, ζ, a (or f_{co}), Q_o, ηf_c, L and I_o. For each set of these parameters, pairs of values for Q_x and the start oscillation frequency f_{so} are successively guessed and the gain is calculated. When a pole in the gain is achieved (in practice a gain in excess of 100 is accepted), the set of parameter values is taken to be the start oscillation condition. Although this is trial-and-error procedure, the parameter range for oscillation is

limited, and experience enables start oscillation conditions to be attained within a few tries. Thus, in practice the procedure is rapid and not expensive in computer time.

For a given value of the d-c magnetic field there is only a limited range of cavity length which will produce oscillation. It is possible to optimize the combination of ηf_c and L for fixed values of the other parameters to produce start oscillation for the minimum Q_L. In general, this optimization was not attempted in this investigation. Most of the calculations were made with a cavity length L such that the cavity TE_{101} resonance occurred at a frequency $f_o = 1.01\ f_c$. However, it became apparent in the study that a more optimum value would have been with L such that $f_o = 1.005\ \eta f_c$, and some data were taken with this value.

All of the data presented in Figures 3 through 7 are for $\sigma = 0.01$, $\zeta = 0.20$, and $f_{co} = 9$ GHz ($a = 1.6655$ cm).

3. Start oscillation conditions

Figure 3 shows the start oscillation beam current I_o versus Q_L with L/a as a parameter for $f_o = 1.01\ \eta f_c$. Note that the various curves are nearly straight lines. It is found that in the range $0.9<L/a<1.5$, I_o varies approximately as $1/Q_L$ in agreement with experiment.[4] For $L/a<0.9$, I_o decreases more rapidly, and for $L/a>1.5$, I_o decreases more slowly than $1/Q_L$. Limited calculations of I_o versus Q_L for a cavity with $f_{co} = 90$ GHz gave results which coincided with the curves shown for $f_{co} = 9$ GHz. It is presumed that the results obtained here can be scaled throughout the microwave and millimeter wavelength range.

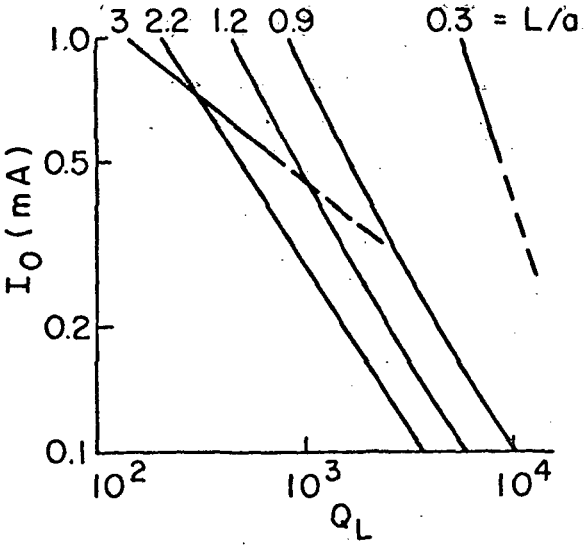

Figure 3. Start oscillation d-c beam current I_o versus Q_L ($f_o = 1.01\ \eta f_c$).

The influence of the axial velocity parameter σ was briefly examined. For $I_o = 1.0$ mA, $L/a = 2.2$, and $\zeta = 0.20$, calculations for $\sigma = 0.02$ and 0.03 were made. It was found that for $\sigma = 0.02$, the start oscillation Q_L was increased by a factor of five, while for $\sigma = 0.03$, no start oscillation condition could be achieved. Thus, we conclude that the start oscillation conditions are a sensitive function of the axial drift velocity.

Figure 4 shows the start oscillation current I_o versus Q_L for the same beam and cavity parameters as Figure 3, but with $f_o = 1.005\ \eta f_c$. Note that the general shape of the curves is similar

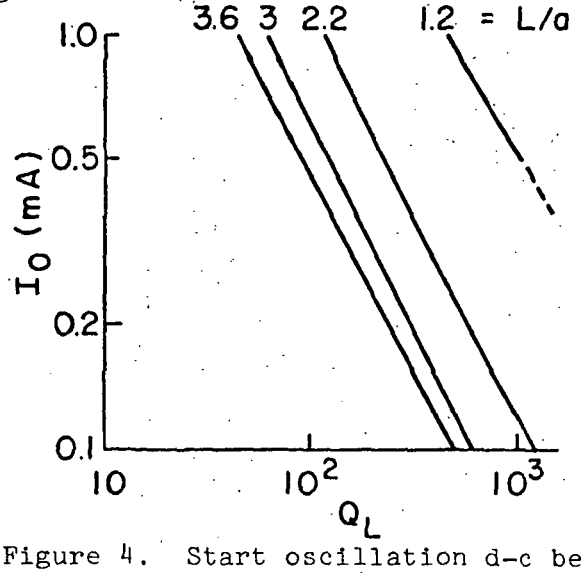

Figure 4. Start oscillation d-c beam current I_o versus Q_L ($f_o = 1.005\ \eta f_c$).

to the previous figure, but the curves are shifted to lower values of Q_L. These curves, together with other calculations, indicate that this combination of L/a and nf_c is nearly optimum.

For reference, Figure 5 shows the variation of the start oscillation frequency with cavity length, plotting f_{so}/f_{co} versus L/a. This curve is only approximate, since there is some frequency pushing as I_o is varied, and also the oscillation frequency shifts slightly as nf_c is varied at fixed L/a.

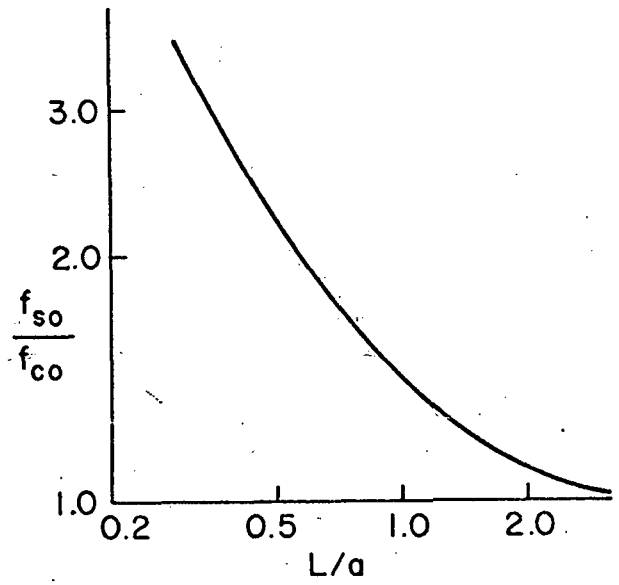

Figure 5. Ratio of start oscillation frequency to waveguide cutoff frequency, f_{so}/f_{co}, versus ratio of cavity length to width, L/a.

However, these effects are negligible on the scale of this figure. Note that start oscillation calculations have been made over a frequency range of about three to one.

Figure 6 shows curves of L/a versus Q_L at start oscillation with the d-c beam current I_o as the parameter for $f_o = 1.01\ nf_c$. For $I_o \lesssim 0.5$ mA, there is an optimum value for L/a for which the Q_L at start oscillation is minimum. For $I_o = 0.1$ mA, start oscillation conditions are obtained only for $0.5 \lesssim L/a \lesssim 3$. For $I_o \gtrsim 0.8$ mA, there is apparently no optimum value for L/a, and as L/a is increased, Q_L for start oscillation decreases monotonically. Thus at a d-c beam current between 0.5 and 0.8 mA, the character of the curves changes.

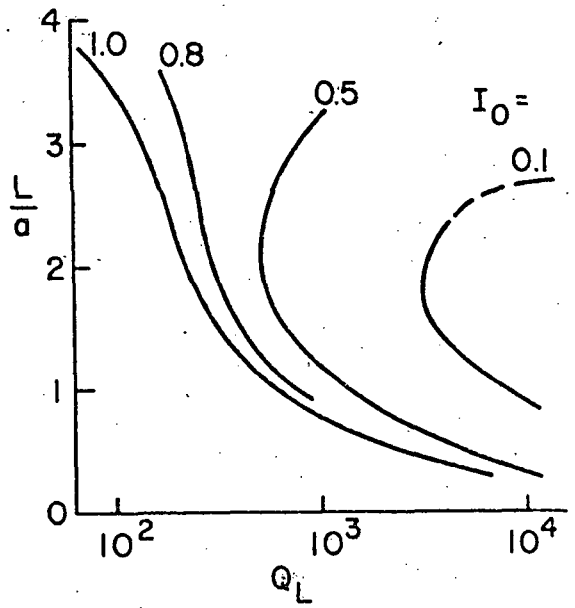

Figure 6. Ratio of cavity length to width, L/a, versus Q_L, at start oscillation ($f_o = 1.01nf_c$).

Figure 7 shows curves of L/a versus Q_L at start oscillation for $f_o = 1.005\ nf_c$. Note that these curves

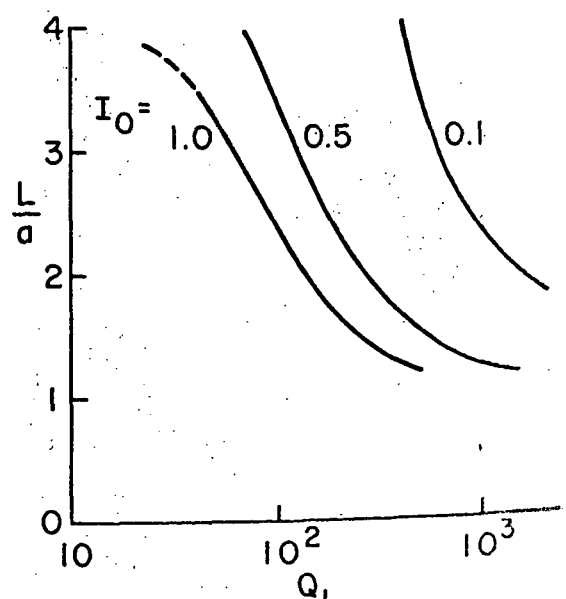

Figure 7. Ratio of cavity length to width, L/a, versus Q_L at start oscillation ($f_o = 1.005nf_c$).

are shifted upward toward higher values of Q_L compared to the curves in Figure 6. This again indicates that this combination of L/a and ηf_c is more *nearly optimum for start oscillation* of the cyclotron resonance oscillator at a given d-c beam current.

All the curves in Figure 7 show a monotonic decrease of Q_L as L/a is increased. That is, no optimum value of L/a exists, at least for $0.1 \lesssim I_o \lesssim 1.0$ mA, and these curves are all similar to the curves in Figure 6 for the larger beam currents $I_o \gtrsim 0.8$ mA. This suggests that the change in the character of the curves in Figure 6 as the d-c beam current is decreased is caused by the non-optimum combination of L/a and ηf_c. For the optimum combination of L/a and ηf_c, start oscillation can presumably be achieved down to low values of Q_L for low values of d-c beam current by increasing L/a; that is, by operating close to the cutoff frequency f_{co} of the waveguide. Reference to the coupled mode theory[5] shows that the coupling parameter involves the waveguide impedance which approaches infinity at f_{co} for TE modes. However, if the combination of L/a and ηf_c is not optimum, then the range of beam currents for which start oscillation at low values of Q_L can be achieved is limited. In this case one finds a beam current level below which only a minimum value of Q_L can be obtained at a finite value of L/a, as shown by the curves in Figure 6 for $I_o \lesssim 0.5$ mA. There is some indication that the start oscillation conditions may change for very large values of L/a, but this has not yet been explored.

The sensitivity of the start oscillation frequency to the d-c beam current can be determined by comparing the start oscillation frequency f_{so} to the upper intersection frequency f_u on the ω-β diagram for the beam-circuit system *in the limit of zero coupling*. It is found that for the optimum combination of L/a and ηf_c (i.e., $f_o = 1.005\ \eta f_c$), $|\Delta f| \lesssim 0.002\ f_u$, where $\Delta f = f_{so} - f_u$. For large values of L/a (e.g., L/a $\gtrsim$ 3), Δf is positive and decreases with increasing beam current. For smaller values of L/a, Δf increases with increasing beam current; in this range Δf is positive for moderate values of L/a and negative for small values (e.g., L/a $\lesssim$ 1.5). It is estimated that a value of L/a between 2.5 and 3 will produce a start oscillation frequency that is approximately independent of the d-c beam current in the range from 0.1 to 1.0 mA.

4. Acknowledgment

The authors wish to thank NASA, Electronics Research Center, Cambridge, Massachusetts, for their support of this work.

References

1. Hirshfield, J.L. and Wachtel, J.M., Electron Cyclotron Maser, Phys. Rev. Letters, 12, 533, 1964.
2. Bott, I.B., A Powerful Source of Millimetre Wavelength Electromagnetic Radiation, Physics Letters, 14, 293, 1965.
3. Beasley, J.P., An Electron Cyclotron Resonance Oscillator at Millimetre Wavelengths, Proc. 6th Int. Conf. on Microwave and Optical Generation and Amplification, 132, Cambridge, 1966.
4. Kulke, B. and Wilmarth, R.W., Small-Signal and Saturation Characteristics of an X-band Cyclotron-Resonance Oscillator, Proc. IEEE, 57, 219, 1969.

5. McIsaac, P.R., Spiraling Electron Beam Interaction with Fast Wave Circuits, Proc. 7th Int. Conf. on Microwave and Optical Generation and Amplification, 253, Hamburg, 1968.

APPENDIX III

SATURATION EFFECTS IN CYCLOTRON RESONANCE OSCILLATORS

J. F. Rowe, Jr.

(International Journal of Electronics,
31, No. 1, 33-45, 1971)

INT. J. ELECTRONICS, 1971, VOL. 31, NO. 1, 33–45

Saturation effects in cyclotron resonance oscillators†

J. F. ROWE, JR.‡
School of Electrical Engineering, Cornell University,
Ithaca, New York 14850

[Received 19 January 1971]

This paper presents the results of a large signal analysis of a cyclotron resonance oscillator. A digital computer was used to obtain numerical results for a particular set of parameters. The model adopted for the oscillator assumes a spiralling filamentary electron beam interacting with a rectangular cavity. Both the gain and saturation mechanisms for a cylotron resonance oscillator are discussed.

List of principal symbols

a	waveguide width.
B_0	d.c. axially directed magnetic field.
$\mathbf{B}$	total r.f. magnetic field.
c	velocity of light.
e	charge of electron.
$\mathbf{E}$	total r.f. electric field.
E_0	peak r.f. electric field strength in dielectric.
I_0	d.c. beam current.
$\mathbf{J}$	current density vector.
k_1, k_2	propagation constants.
m_0	electron rest mass.
Q_x	external Q.
R	energy balance factor.
t	time.
U	impedance mismatch factor.
$\mathbf{v}$	total beam velocity.
V_0	d.c. beam voltage.
$v_{nx,\,y,\,z}$	nth order Fourier components for x, y, and z velocities.
v_{t0}	transverse velocity
x, y, z	rectangular coordinate system.
x', y'	$(x+a/2)$, $(y+a/2)$.
v_{z0}	axial velocity.
Z_1, Z_2	waveguide impedances.
β_c	beam cyclotron wave number.
ϵ_0	permittivity of free space.
ϵ_r	relative permittivity of dielectric.
η	impedance of free space $=(\mu_0/\epsilon_0)^{1/2}$.
$\dot{\theta}$	relativistic orbiting radian frequency.

† Communicated by Dr. P. A. Lindsay.

‡ Present address: Watkins Johnson Company, CEI Division, 6006 Executive Boulevard, Rockville, Maryland 20852, U.S.A.

λ r.f. field wavelength in cavity.
μ_0 permeability of free space.
ρ total charge density.
τ_n nth order Fourier component in charge density expansion.
ψ conversion efficiency.
ω r.f. radian frequency.
ω_{c0} waveguide radian cut-off frequency in TE_{10} mode $= \pi c/a$.

1. Introduction

Over the past decade much attention has been focused upon devices utilizing the interaction of fast waves with rotating electron beams. Tubes based on this principle, the ' Electron Cyclotron Masers ' or 'Cyclotron Resonance Oscillators ', have potential as generators of high power millimetre wavelength radiation. A sequence of such devices has been constructed and reported upon : Chow and Pantell (1960), Hirschfield and Wachtel (1964), Bott (1964), Beasley (1966), Antakov *et al.* (1966), Schriever and Johnson (1966), and Kulke (1969).

It was shown by Chow and Pantell (1960) that the interaction of rotating charge with the transverse waveguide magnetic field can produce longitudinal bunching and set up conditions for energy transfer to the electromagnetic fields via the $\mathbf{v} \cdot \mathbf{E}_{r.f.}$ mechanism. Subsequently, Hsu (1966) discovered that the beam-field coupling produces a relativistic electron mass shift which leads to wave growth. Sehn and Hayes (1969) compared the effects of relativistic bunching and transverse magnetic field bunching and concluded that in the hollow beam–TE_{10} waveguide mode interaction, relativistic bunching predominates, particularly near cut-off. Lindsay (1970) supports this conclusion in the case of helical, filamentary beams, and presents evidence that the r.f. magnetic fields in fact always oppose the relativistic growth mechanism for the forward-wave interaction.

A small signal coupled-mode analysis describing the interaction of a spiralling, filamentary electron beam with the fields of a uniform waveguide has been developed by McIsaac (1968) and extended to predict the start-oscillation conditions of a device with the beam inside a rectangular cavity (McIsaac and Rowe 1970). The model utilizes a filamentary helix of charge with electrons drifting along the cavity axis with axial velocity v_{z0} and rotating about a static magnetic field B_0 with transverse velocity v_{t0} at radian frequency

$$\theta = \frac{eB_0}{m_0}\left[1 - \frac{(v_{t0}^2 + v_{z0}^2)}{c^2}\right]^{1/2} \tag{1}$$

With the electron orbiting frequency set slightly below cavity resonance, strong coupling between the electron beam and the electromagnetic field occurs, and self-sustaining oscillations are produced. It is found that to obtain oscillations, practically all the beam energy must be incorporated in kinetic energy of rotation.

With the intent of further illuminating the processes at work within cyclotron resonance devices, this paper presents a large signal ballistic analysis of a spiralling, filamentary electron beam interacting with the r.f. fields of a rectangular, lossless cavity of square cross section. Space-charge forces have been neglected, and only the effects of the dominant, degenerate, TE_{101} and TE_{011}

modes are considered. The beam radius r_0 is much less than the cavity width. As a consequence, the presence of the axial component of the r.f. magnetic field is ignored, and the transverse r.f. fields are assumed to be circularly polarized, rotating in the same sense as the charge.

The fields within the cavity satisfy the non-homogeneous wave equations:

$$\nabla^2\mathbf{E} - \frac{1}{c^2}\frac{\partial^2\mathbf{E}}{\partial t^2} = \frac{\nabla\rho}{\epsilon_0} + \mu_0\frac{\partial\mathbf{J}}{\partial t}, \tag{2}$$

$$\nabla^2\mathbf{B} - \frac{1}{c^2}\frac{\partial^2\mathbf{B}}{\partial t^2} = -\frac{\nabla\times\mathbf{J}}{\mu_0}. \tag{3}$$

The homogeneous solutions to these equations are given by the familiar cavity standing-wave fields. Upon introduction of an electron beam into the structure a non-homogeneous or 'driven' solution appears and must be superimposed upon the homogeneous solution to obtain the total field.

The motion of charge within the cavity is governed by the relativistic equation of motion :

$$\frac{d}{dt}\left\{\frac{\mathbf{v}}{\left[1-\left(\frac{|\mathbf{v}|^2}{c^2}\right)\right]^{1/2}}\right\} = \frac{e}{m_0}[\mathbf{E}+\mathbf{v}\times\mathbf{B}+\mathbf{v}\times B_0\mathbf{a}_z], \tag{4}$$

where B_0 is the axial d.c. magnetic flux density which produces the spiralling motion of the d.c. beam.

Fig. 1

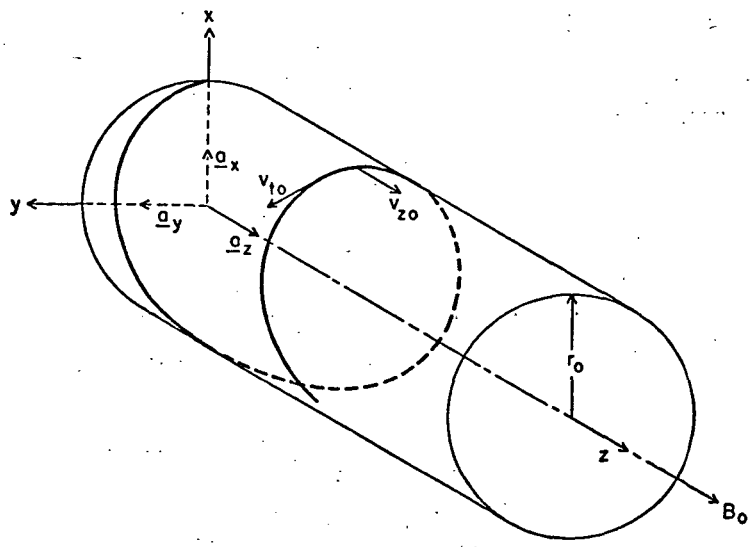

Beam geometry.

In the analysis the continuous beam of fig. 1 is decomposed into a series of discrete charge groups. The Cyclotron Resonance Oscillator is assumed to have settled into steady-state operation, i.e.

$$f\left(t+\frac{m2\pi}{\omega}\right)=f(t), \quad m=\pm 1, \pm 2, \ldots \tag{5}$$

for all beam and field quantities, and only those representative charge groups entering the structure over one r.f. cycle need be considered.

Based upon the fields within an infinite waveguide with a step dielectric discontinuity, a model of the cavity has been devised and will be described in the next sections. With a modulated electron beam in the waveguide, it is possible to generate a condition of zero transverse electric field at a point one-half wavelength distant from the discontinuity. The waveguide can thus be shorted and converted into a resonant cavity.

The helical beam enters the cavity and is acted upon by the homogeneous r.f. fields. The beam becomes distorted as position modulation appears. A Fourier analysis of beam variables is performed at periodically spaced axial intervals, and based upon certain 'slowly varying' assumptions on the Fourier coefficients, approximate closed-form expressions for the non-homogeneous fields can be generated. In this manner the charge-group equations of motion are integrated along the length of the cavity. Oscillation conditions require the maintenance of boundary conditions at both the entrance and exit planes; if these are fulfilled, then the input parameters are consistent with oscillation. However, if the requisite final conditions are not satisfied at the cavity exit, the initial parameters are reset and the integrations repeated until oscillation conditions are achieved.

2. Cavity standing-wave patterns

The magnitude of the TE_{101}, standing-wave, transverse electric and magnetic fields of a lossless, closed, rectangular cavity are sketched in fig. 2 (*a*). Since the tangential components of E must be zero at the end walls, the electric field exhibits the well-known $\sin(2\pi z/\lambda)$ form.

With a spiralling electron beam in the cavity, non-homogeneous electric fields are generated. The transverse field components must still vanish at the

Fig. 2

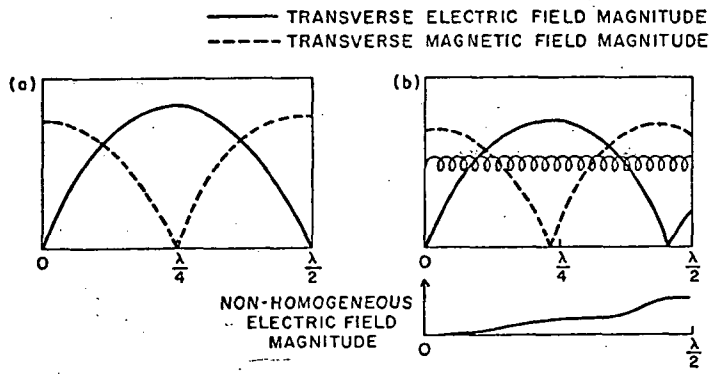

(*a*) 'Cold' resonance standing-wave patterns; (*b*) excited standing-wave patterns.

end walls. To yield the required cancelling field, there must be some shift in the resonant frequency of the cavity (fig. 2 *b*).

With this simple physical argument as a point of reference, the fields within an inhomogeneously filled waveguide will be examined and used to produce an idealized cavity model.

3. Cavity model

A lossless waveguide of square ($a \times a$) cross section is evacuated in the region $z > 0$ and filled with a lossless, non-magnetic dielectric of relative permittivity ϵ_r for $z < 0$. In the evacuated portion, the impedance of the degenerate TE_{10} and TE_{01} modes is

$$Z_1 = \frac{\eta}{\left[1 - \left(\frac{\omega_{co}}{\omega}\right)^2\right]^{1/2}}, \tag{6}$$

and in the dielectric,

$$Z_2 = UZ_1. \tag{7}$$

Such a model is not proposed as being representative of any physical device. This model does allow the large signal interaction within the cavity to be readily analysed, including the effects of external loading. It is believed, moreover, that this large signal analysis should be applicable to the interpretation of the interaction in actual cyclotron resonance devices with cavities employing an output system of vacuum window and iris, if the Q_x of the model employed here is adjusted to equal the value for the device.

An r.f. wave comprised of equi-amplitude, and $\pi/2$-phased, TE_{10} and TE_{01} modes propagates in the $-z$ direction and strikes the discontinuity at $z = 0$. The transverse components of the transmitted fields in the dielectric ($z < 0$) are written as

$$E_{2x} = E_0 \sin\frac{\pi y'}{a} \cos(\omega t + k_2 z), \tag{8}$$

$$E_{2y} = E_0 \sin\frac{\pi x'}{a} \sin(\omega t + k_2 z), \tag{9}$$

$$H_{2x} = \frac{E_{2y}}{Z_2}, \tag{10}$$

$$H_{2y} = -\frac{E_{2x}}{Z_2} \tag{11}$$

with

$$k_2 = \frac{\omega \epsilon_r^{1/2}}{c}\left[1 - \left(\frac{\omega_{co}}{\epsilon_r^{1/2}\omega}\right)^2\right]^{1/2}. \tag{12}$$

This wave is the output from the oscillator.

Relative to the transmitted, or ' output ' field magnitude E_0, the transverse fields in the region $z>0$ are

$$E_{1x}=\frac{E_0(U+1)}{2U}\sin\frac{\pi y'}{a}\left[\cos(\omega t+k_1z)+\left(\frac{U-1}{U+1}\right)\cos(\omega t-k_1z)\right], \quad (13)$$

$$E_{1y}=\frac{E_0(U+1)}{2U}\sin\frac{\pi x'}{a}\left[\sin(\omega t+k_1z)+\left(\frac{U-1}{U+1}\right)\sin(\omega t-k_1z)\right] \quad (14)$$

and

$$H_{1x}=\frac{E_0(U+1)}{2UZ_1}\sin\frac{\pi x'}{a}\left[\sin(\omega t+k_1z)-\left(\frac{U-1}{U+1}\right)\sin(\omega t-k_1z)\right], \quad (15)$$

$$H_{1y}=-\frac{E_0(U+1)}{2UZ_1}\sin\frac{\pi y'}{a}\left[\cos(\omega t+k_1z)-\left(\frac{U-1}{U+1}\right)\cos(wt-k_1z)\right] \quad (16)$$

with

$$k_1=\frac{\omega}{c}\left[1-\left(\frac{\omega_{co}}{\omega}\right)^2\right]^{1/2}. \quad (17)$$

On the waveguide axis, the r.f. fields are circularly polarized.

The fields of eqns. (13)-(16) are the superposition of the forward and reverse homogeneous transverse solutions to the wave equations. Acted upon by these fields, the beam response is described by Fourier expansions :

$$v_x(z,t)=\sum_{n=0}^{\infty}v_{nx}(z)\exp[jn(\omega t-\beta_c z)], \quad (18)$$

$$v_y(z,t)=\sum_{n=0}^{\infty}v_{ny}(z)\exp[jn(\omega t-\beta_c z)], \quad (19)$$

$$v_z(z,t)=\sum_{n=0}^{\infty}v_{nz}(z)\exp[jn(\omega t-\beta_c z)]. \quad (20)$$

The wave number β_c is defined by the integral

$$\beta_c(z)=\frac{\omega}{2\pi}\frac{eB_0}{m_0}\frac{1}{v_{z0}(z)}\int_0^{2\pi/\omega}\left[1-\frac{v^2(z,t)}{c^2}\right]dt. \quad (21)$$

This quantity represents the time-averaged propagation ' constant ' of spiralling electrons as a function of the axial coordinate.

Because of charge gyration about B_0, the x and y Fourier coefficients are approximately space-periodic and are taken as

$$v_{nx}(z)=u_{nx}(z)[-\sin(\beta_c z+\phi)], \quad (22)$$

$$v_{ny}(z)=u_{ny}(z)\cos(\beta_c z+\phi). \quad (23)$$

The charge-density function is described by

$$\rho(z,t)=\delta(x)\delta(y)\left\{\left[\frac{I_0}{v_{z0}(z)}+\sum_{n=1}^{\infty}\tau_n(z)\exp[jn(\omega t-\beta_c z)]\right]\right\}. \quad (24)$$

The δ functions arise from the filamentary nature of the beam. Since the charge orbiting radius is small compared to the waveguide width, the charge location is approximated as the centre of the waveguide ; this simplifies the calculation of the interaction and is consistent with the other approximations made.

The quantities u_{nx}, u_{ny}, v_{nz}, β_c, $\dot{\phi}$, and τ_n are all 'slowly varying' functions of the axial coordinate. Thus, over appropriately short distances they can be treated as constant and their derivatives neglected. Substitution of the Fourier expansions into the right-hand side of the wave eqns. (2), (3) yields tractable expressions for the non-homogeneous fields, and completes the self-consistency loop. In the analysis, only terms to order 2ω are retained.

Fig. 3

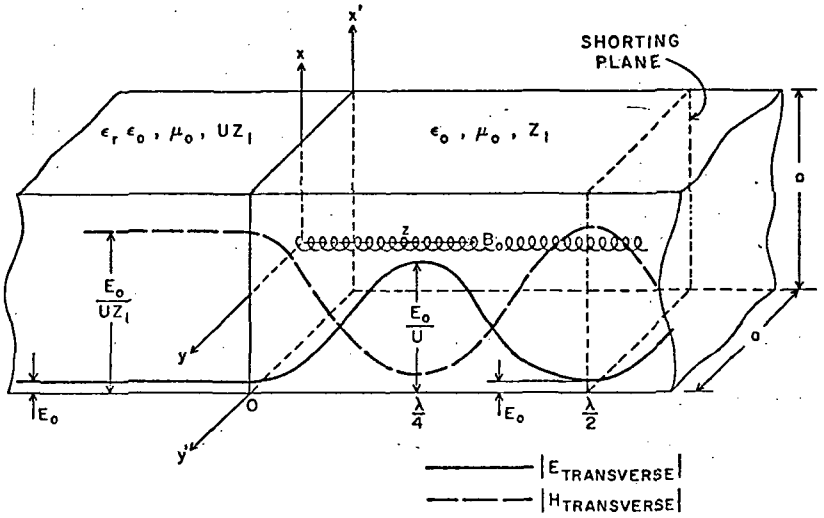

Cavity model and standing-wave pattern.

If the transverse non-homogeneous electric field is equal in magnitude and opposite in phase to the transverse homogeneous electric field at the first standing-wave minimum at $z=\lambda/2$, a shorting plane can be introduced and a closed, resonant structure is formed. This condition is imposed as one of the boundary conditions which must be satisfied in the oscillator. Using the definition of 'external Q',

$$Q_x = \frac{\omega \text{ (stored energy)}}{\text{power out}}, \tag{25}$$

it is found that for this half-wavelength cavity,

$$Q_x = \frac{\omega \epsilon_0 \lambda Z_1}{4U}. \tag{26}$$

Fixing the beam kinetic power (VI_0), the strength of the cavity fields is varied by altering the conversion efficiency

$$\psi = \frac{\text{r.f. power coupled out through dielectric}}{\text{beam kinetic power}} = \frac{\frac{E_0^2 a^2}{2Z_1 U}}{VI_0}. \tag{27}$$

Finally, an energy balance factor

$$R(z)=\frac{\text{(initial beam kinetic power)—(beam kinetic power at } z)}{\text{r.f. power coupled out through dielectric}} \tag{28}$$

is monitored throughout the length of the cavity. Oscillation conditions require the simultaneous existence of two boundary conditions :

$$R(\lambda/2)=1{\cdot}0 \tag{29}$$

$$E_{\text{transverse}}(\lambda/2)=0. \tag{30}$$

4. Computational aspects

The system of the equations of motion (one for each charge group) and wave equations was solved on an IBM 360 digital computer. The cavity and beam parameters were selected to conform as closely as possible to those given by Kulke (1969) for his tube, and are summarized below :

waveguide cut-off frequency	6·56 GHz
cyclotron orbiting frequency	9·35 GHz
beam voltage	15 kv
beam current	5·5 mA
axial velocity	0·0181c
transverse velocity	0·236c
unmodulated beam diameter/waveguide width ..	0·105

The beam was represented by eight charge groups entering the cavity at intervals of $\pi/4$ in r.f. phase.

5. Results

Due to uncertainties as to what fraction of the cathode current entered into the interaction process, exact values of saturation beam current for the Kulke oscillator are not available. The tube produced peak power at a loaded Q of 640 and a beam current thought to be about 5·5 mA. At this point, the oscillator efficiency approached 4%. With these parameters as a guide, the model was employed to study oscillator performance at saturation.

With the conversion efficiency set at 1·2%, well below the anticipated saturation level, a sequence of computer runs was made at the 5·5 mA beam current level, while the external Q was varied. As shown in fig. 4, the energy conservation condition of eqn. (29) is satisfied for $Q_x=351$. The driven r.f. electric fields at this efficiency level were found to be twice as large as the standing-wave electric field minimum (fig. 5). Holding Q_x fixed at 351, another series of computer runs was made for increasing efficiency levels in order to find the efficiency yielding the short-circuit condition of eqn. (30). Slight alterations in frequency were necessary at each step to satisfy eqn. (29).

Under the influence of the strong transverse r.f. magnetic field at the cavity entrance, axial accelerations produced charge-group crossovers a short way into the structure. Beyond the crossover points, the Fourier expansions of

Fig. 4

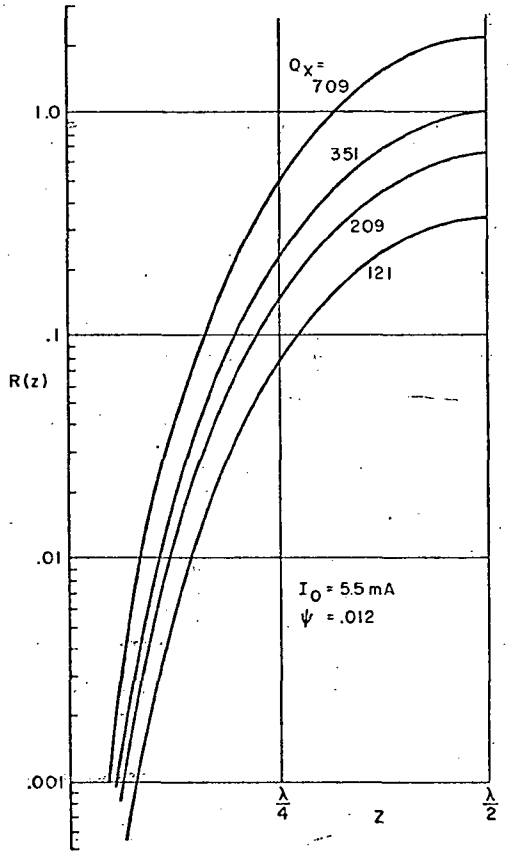

Energy balance factor versus axial distance.

Fig. 5

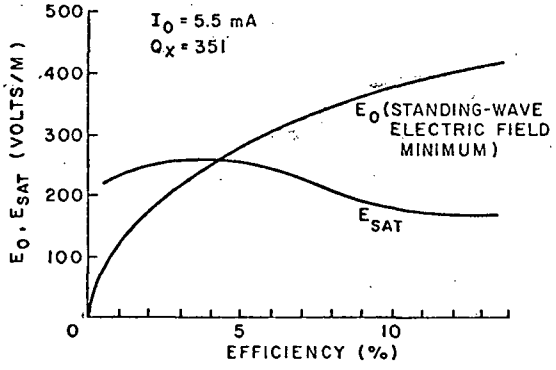

Transverse electric field magnitudes at the $\lambda/2$ point versus efficiency. E_{SAT} is the amplitude of the non-homogeneous electric field at $z=\lambda/2$.

eqns. (18)–(20) become invalid as beam velocities are no longer single-valued functions of the axial coordinate. In the face of the extremely non-linear beam response, information on the non-homogeneous field magnitudes must be interpreted with care since these fields are constructed from Fourier coefficients. In spite of the questionability of the Fourier expansions, the analysis was continued beyond the crossing points and led to an interesting and plausible saturation mechanism. Although the computed values of the non-homogeneous field are dubious, this will not significantly affect the calculation of the charge motion since the non-homogeneous electric fields are very small compared to the homogeneous electric field except near $z=\lambda/2$.

For assumed efficiency levels as high as 13%, frequency alterations could be made to maintain the energy conservation requirement of eqn. (29). But, as indicated in fig. 5, the limitation on efficiency seems to be set by the inability of the non-homogeneous electric fields to cancel the homogeneous electric field at the standing-wave minimum. Thus the short-circuit condition of eqn. (30) could not be satisfied. The interaction point in fig. 5 where the non-homogeneous and homogeneous electric fields are equal occurs in the $4\frac{1}{2}$%–5% efficiency range. With this evidence locating the point of saturation, tube conditions at 5% efficiency were examined in detail.

In fig. 6 the magnitude of the homogeneous transverse standing-wave electric field component is superimposed over the function $(d/dz)R(z)$ which describes the spatial distribution of the power flux from the beam to the electromagnetic fields.

Fig. 6

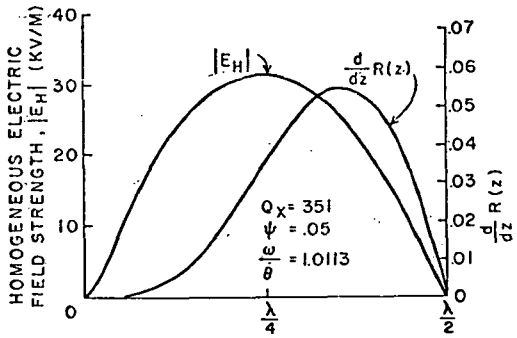

Axial rate of change of the energy balance factor, $(d/dz)R(z)$, versus axial position in the cavity.

It is significant that the power exchange is rising rather sharply at the cavity midpoint where the transverse r.f. magnetic field is at a minimum. If the r.f. magnetic field were the primary bunching mechanism, the power exchange would level off at the $\lambda/4$ midpoint where B is minimum. The fact that it does not, points to the relativistic mass shift as the predominant gain mechanism.

The velocity profiles of the representative charge groups in their flight through the cavity are shown in figs. 7 and 8. It is noted that the maximum increase in transverse velocity gained by beam electrons is about 13%. Since

Fig. 7

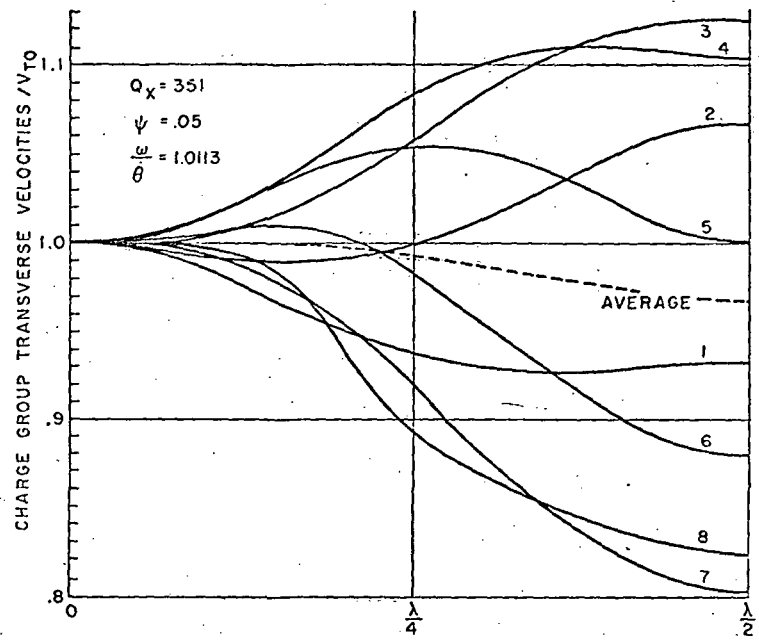

Transverse velocities of the eight charge groups (normalized to the initial d.c. transverse velocity v_{to}) versus axial position in the interaction cavity.

Fig. 8

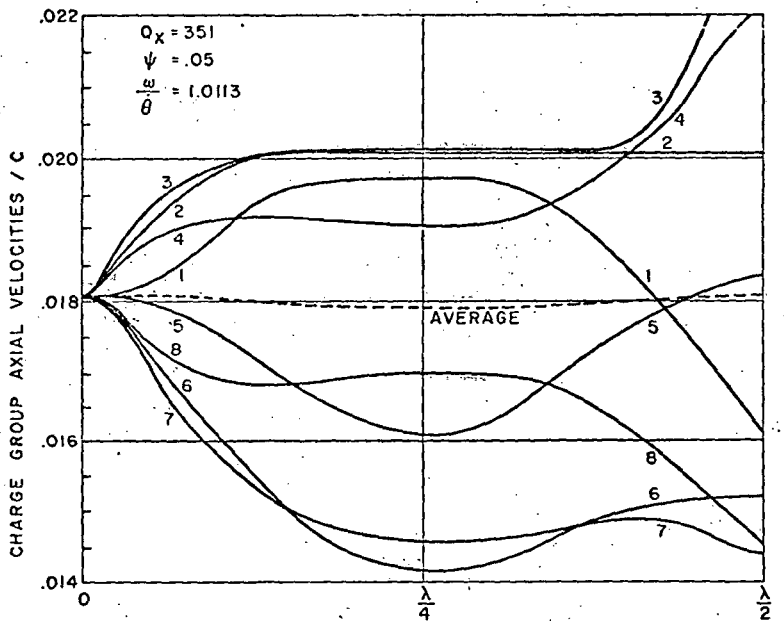

Axial velocities of the eight charge groups (normalized to the velocity of light) versus axial position in the interaction cavity.

these electrons increase their orbiting radius proportionately, the entire beam remains confined close to the waveguide axis and, at least for the parameters used, collection of charge by waveguide walls does not occur.

The dashed line of fig. 7 shows how the averaged transverse velocity of the beam decreases along the cavity as energy is given to the r.f. fields. By eqn. (1), the average cyclotron frequency is greater than that of the unmodulated beam, and it is anticipated that the oscillation frequency will be above that of the 'cold' resonance. Further, the amount of upward frequency shift is limited by beam saturation effects as discussed in § 2. Steady-state operation sets in at the efficiency level where the saturated beam field matches and cancels the off-resonance field at the output wall (fig. 2 *b*).

It is noted that the averaged axial velocity in fig. 8 tends to remain approximately constant over the entire cavity length. Since energy conversion is at the expense of rotational energy, it is desirable to utilize beams having a high ratio of transverse velocity to axial velocity.

6. Conclusion

For X-band frequencies and easily realizable beam parameters, efficiencies on the order of 4–5% are predicted for the interaction of a spiralling electron beam with a half-wavelength resonant cavity. This prediction agrees favourably with the observed behaviour of an existing device (Kulke 1969).

This large signal analysis indicates that the major gain mechanism in the cyclotron resonance oscillator is associated with the bunching produced by changes in mass of the velocity modulated electrons. This effect predominates over the bunching caused by the r.f. magnetic field. Because the gain mechanism is relativistic in nature, angular velocities of the order of $0{\cdot}1c$ must be obtained in the interaction cavity to obtain oscillation.

Essentially, as the output power increases from the start-oscillation condition to the saturated level, the oscillation frequency changes (slightly) to produce the required phase characteristic of the cavity fields relative to the spiralling electron beam. The output power increases until the frequency change is so large that the non-homogeneous r.f. electric field produced by the modulated electron beam can no longer cancel the homogeneous r.f. electric field at the collector end of the cavity. At this point, saturation is reached.

The interaction of a spiralling electron beam with a microwave cavity generates intense r.f. fields which produce strong axial velocity modulation of beam electrons. The electron beam response is extremely non-linear. Electron cross-overs occur within the cavity and a rigorous analysis must account for the multi-valued velocity functions produced on the electron beam.

Acknowledgments

This work is part of a Ph.D. thesis at Cornell University, supported by the NASA Electronics Research Center, Cambridge, Massachusetts, and guided by Professor Paul R. McIsaac. I remain indebted to Professor McIsaac for the years of direction and aid.

References

Antakov, I. I., Gaponov, A. V., Malygin, O. V., and Flyagin, V. A., 1966, *Radio Engng electron. Phys.*, **11**, 106.

Beasley, J. P., 1966, Proc. Sixth Int. Conf. Microwave and Optical Generation and Amplification, Cambridge.

Bott, I. B., 1964, *Proc. I.E.E.E.*, **52**, 330.

Chow, K. K., and Pantell, R. H., 1960, *Proc. Inst. Radio Engrs*, **48**, 1965.

Hirshfield, J. L., and Wachtel, J. M., 1964, *Phys. Rev. Lett.*, **12**, 533.

Hsu, T. W., 1966, Ph.D. Thesis, Sheffield.

Kulke, B., 1969, "Design Considerations for Cyclotron Resonance Oscillators", NASA TN D-5237.

Lindsay, P. A., 1970, Proc. Eighth Int. Conf. Microwave and Optical Generation and Amplification, Amsterdam.

McIsaac, P. R., 1968, Proc. Seventh Int. Conf. Microwave and Optical Generation and Amplification, Hamburg.

McIsaac, P. R., and Rowe, J. E. Jr., 1970, Proc. Eighth Int. Conf. Microwave and Optical Generation and Amplification, Amsterdam.

Schriever, R. L., and Johnson, C. C., 1966, *Proc. I.E.E.E.*, **54**, 2029.

Sehn, G. J., and Hayes, R. E., 1969, *I.E.E.E. Trans. electron Devices*, **16**, 1077.